Journal of Current Research in Oral Surgery
2026, Volume 6, Issue 1, Page No: 162-171

Available online at: www.tsdp.net

ISSN: 3062-3480

Original Article

Virtual Planning and Patient-Specific Implant Design for Secondary Reconstruction of Malaligned Zygomatic Fractures

Juan Perez[1], Ana Gutierrez[1]*, Carlos Lopez[2]

[1]Department of Oral and Maxillofacial Surgery, Faculty of Dentistry, National Autonomous University of Mexico, Mexico City, Mexico.
[2]Department of Clinical Oral Sciences and Dental Surgery, Faculty of Medicine, Monterrey Institute of Technology, Monterrey, Mexico.

***E-mail** ✉ ana.gutierrez@gmail.com

Received: 21 February 2026; **Revised:** 17 May 2026; **Accepted:** 21 May 2026

ABSTRACT

The zygomatic bone plays a pivotal role in determining the anterior and lateral projections of the midface and the proper placement of the globe. Securing primary anatomical reduction of zygomatic fractures is critical, as secondary reconstruction is substantially more difficult. Addressing a malpositioned zygoma requires osteotomy of the healed bone to facilitate repositioning. Owing to the zygoma's profound influence on midfacial contour, achieving meticulous three-dimensional realignment is paramount. Contemporary technological progress is accelerating, paving the way for enhanced outcomes across a wide array of surgical specialties, and the utilization of bespoke surgical guides and fixation hardware is gaining widespread traction. By applying 3D segmentation and design platforms, we formulated a sequential workflow that leverages three-dimensional planning and additive manufacturing for the refracturing step—circumventing the need for coronal exposure—and for the precise repositioning and stabilization of the zygoma in its corrected location. The methodology is delineated alongside a novel, sophisticated 3D analysis that permits objective evaluation of surgical outcomes. Two clinical cases are detailed, covering both the design phase and the postoperative morphological alterations. A comparative analysis of the preoperative, virtually planned, and final achieved positions revealed a degree of accuracy that effectively eliminates the risk of human error inherent in a three-dimensional-sensitive intervention such as zygomatic refracturing. This protocol lends itself readily to adaptation across other realms of secondary reconstruction, necessitating skeletal realignment.

Keywords: Zygoma, Malar, Refracture, 3D, Patient specific implant, Surgical guide

How to Cite This Article: Perez J, Gutierrez A, Lopez C. Virtual Planning and Patient-Specific Implant Design for Secondary Reconstruction of Malaligned Zygomatic Fractures. J Curr Res Oral Surg. 2026;6(1):162-71. https://doi.org/10.51847/AVf334jESP

Introduction

The projection of the malar eminence renders the zygoma a cornerstone of the middle third of the facial skeleton. Zygomaticomaxillary complex (ZMC) fractures that remain uncorrected or are suboptimally managed can result in both functional impairments and aesthetic disharmony. The belated treatment of a longstanding ZMC fracture typically entails performing releasing osteotomies (refracture) as a prerequisite to repositioning the liberated zygomatic segment. This maneuver demands disarticulation of the zygoma from its articulations with the maxilla, temporal bone, sphenoid bone, and frontal bone. How a chronic or old ZMC fracture is defined remains a matter of discussion, with reported timeframes spanning from several weeks to multiple months across the published literature [1-3]. The operative exposure required for refracturing chronic ZMC fractures typically includes coronal, subciliary, or transconjunctival lower eyelid incisions and intraoral vestibular incisions [4].

Before the introduction of virtual surgical planning, the primary challenge in secondary correction of old ZMC fractures was accurately repositioning the

osteotomized segment. On one hand, the absence of occlusal referencing, and on the other, the progressive bony remodeling along the fracture interfaces, both conspire to render anatomical reduction an arduous task [5]. The emergence of computer-aided design (CAD) and computer-aided manufacturing technologies has enabled preoperative simulation of the proper anatomical location of the refracted segment. Mirror-image superimposition of the unaffected contralateral side onto the traumatized side is a widely adopted virtual technique to facilitate symmetric repositioning [5]. Producing the three-dimensionally planned result as a printed stereolithographic model enables the off-table adaptation and contouring of fixation plates before surgery [6, 7]. Polylactic acid-based materials can be employed to fabricate low-cost osteotomy guides and positioning templates that steer intraoperative bone cuts and segment relocation [8, 9]. The integration of an intraoperative navigational system with computed tomographic data can further enhance the fidelity of the definitive reconstruction and is increasingly regarded as a benchmark of care. However, the associated expenditures remain considerable [4, 6]. In our view, the most cutting-edge deployment of three-dimensional technology in the delayed management of ZMC fractures at present should be the customized design and fabrication of patient-specific implants (PSI) and accompanying surgical guides to achieve both precise and durable repositioning.

Materials and Methods

We performed a retrospective review of individuals who presented with a malpositioned malar bone resulting from a failed primary reduction and who received secondary surgical care at our facility during the 2022–2023 period, employing 3D-printed surgical guides and patient-specific implants. The central goals of this investigation were to formulate a workflow grounded in three-dimensional technology for refracturing and realigning the zygoma through a minimally invasive corridor, and to measure the accuracy delivered by this workflow. Two distinct CAD software packages were used for virtual preparation: the first isolated the anatomical region of interest and generated a 3D STL file **(Figure 1)**, while the second handled malar bone repositioning, surgical guide creation, and PSI blueprinting. Isolation of the area of interest was accomplished with D2P (DICOM to Print) software (3D systems, OR, USA). The subsequent 3D planning was executed in Geomagic Freeform (3D Systems). The foremost difficulty when virtually strategizing these cases is ensuring flawless surface adaptation of the PSI against the refractured and repositioned malar bone once placed in its novel spatial configuration. To satisfy this crucial requirement, we adopted an inverted planning sequence: the PSI was conceptualized first upon the already relocated, refractured malar bone segment, and the surgical guides were designed subsequently.

During this initial step, the drilling perforations intended for PSI fixation—both those seated in the stationary maxillary bone and those within the repositioned zygomatic fragment—are defined according to the ultimate planned position of the refractured malar bone. Two categories of drill perforations exist: those belonging to the mobile fragment and those anchored in the stable facial skeleton. Thereafter, the repositioned zygomatic segment is transposed backward onto its original, pre-planned orientation. This retrograde transfer is conducted together with the drill holes associated with the mobile part, preserving their unchanged spatial orientation relative to the zygomatic segment. Once the malar bone with these drill holes is faithfully restored to its planned location, a drilling template is developed to index all hole positions on both the mobile segment and the stable skeletal framework **(Figure 2)**. As depicted in **Figure 2**, the holes made through the templates will correspond precisely to the perforations of the PSIs only after the malar bone segment has been accurately repositioned, thereby enabling the PSI to serve both as a positioning jig and as a fixation device. These same templates also serve as osteotomy guides for the predetermined bone cuts, allowing intraoral separation of the zygoma and eliminating the need for coronal exposure. Cumulative time expenditure for the segmentation task, the realignment, surgical guide preparation, and patient-specific plate conception averaged 3 hours. A three-dimensional comparison of the preoperative state, the virtually planned position, and the postoperative bony arrangement of the zygoma was performed in CloudCompare (Open source, Freeware). This application uses the Hausdorff distance metric to quantify the deviation between two point cloud sets. Our previously published work delineates this approach to 3D assessment in detail [10]. For soft-tissue appraisal, a 3D PLY file was captured using a soft-tissue scanning device manufactured by Cherry Imaging Ltd (Yokneam, Israel), and the resulting 3D file was subsequently analyzed in CloudCompare.

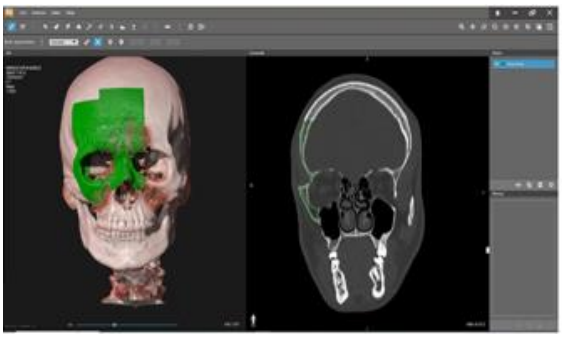

a)

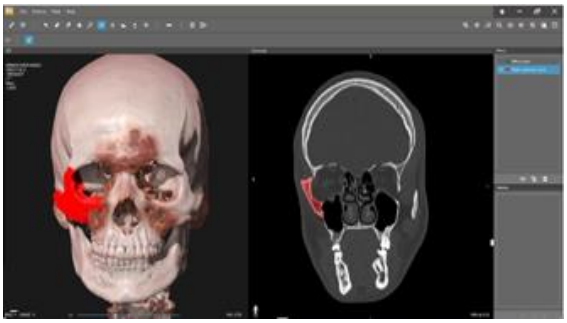

b)

Figure 1. Segmentation: (a) Outline of the targeted region. Every input expands the volume of bone within the outlined zone. Note the three-dimensional display to the left and the coronal display to the right, offering a clearer picture of the precisely outlined territory; (b) The outlined right zygoma after being rendered as a mask. What follows is converting the zygoma into a mesh, then saving it as an STL file to permit further refinement in the 3D design program.

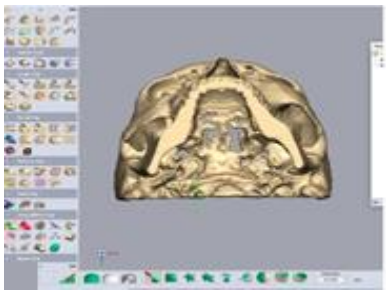

a)

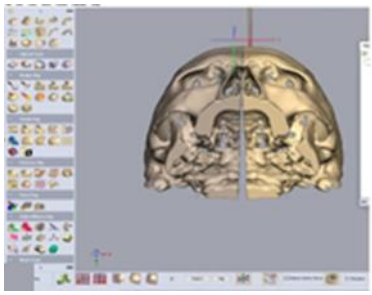

b)

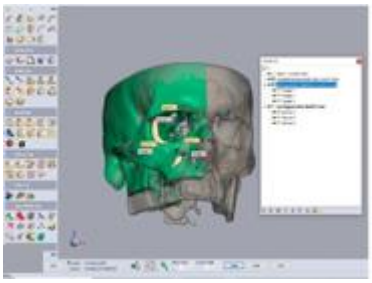

c)

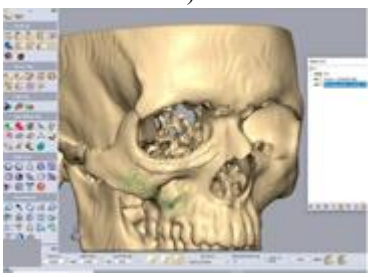

d)

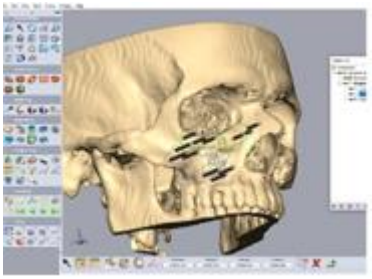

e)

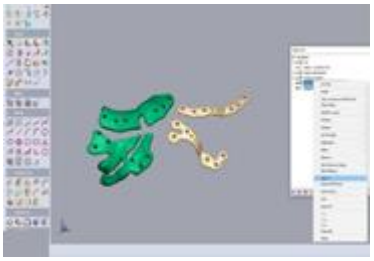

f)

Figure 2. Design phase of zygoma repositioning, surgical guides, and PSI: (a) Upon completing segmentation into an STL file, the planning stage begins using the Geomagic software. The data is brought into the application. Observe how the right zygoma appears depressed when contrasted with the left counterpart; (b) The left zygoma is segmented to enable a mirroring workflow that achieves correct alignment of the impacted right side; (c) The displaced right zygoma is automatically matched to the mirrored left zygoma via multi-point registration; (d) A pair of PSI is engineered to secure the final positioned outcome; (e) Two surgical guides are constructed, serving the dual purpose of guiding the anterior osteotomy and pinpointing drill sites for the final implant placement. Guide-drilled apertures will align with the implant apertures exclusively after the zygoma

has been repositioned exactly as specified in the 3D surgical blueprint; (f) The pair of surgical guides (green) alongside the PSIs.

Results and Discussion

A total of three patients, each with a history of an ineffective prior operative reduction of a zygomatic fracture, who then underwent a revision procedure augmented by 3D technology, were assessed. Preoperatively, every case demonstrated unilateral malar flattening, which was corrected to a considerable degree following the intervention.

The initial stage of the planning pipeline involved zygoma segmentation **(Figure 1)**. **Figure 2a** showcases the depressed contour of the right zygoma after the initial surgery. **Figure 2b** displays the targeted location of the right zygoma, obtained through a mirror-image technique using the contralateral zygoma as the blueprint. **Figure 2c** illustrates the step of aligning the segmented, depressed zygoma to the mirrored template. **Figures 2d and 2e** show the fabrication designs for the PSIs and the cutting jigs, respectively. The openings in the cutting templates correspond to the implants and, consequently, direct the zygoma toward its newly intended spatial orientation. The definitive guides and PSIs are visible in **Figure 2f**. Preoperative and postoperative axial cross-sections generated from stacked CT cuts are shown in **Figures 3a and 3b**, respectively; the symmetry restored by this method is noteworthy. **Figures 3c and 3d** capture the clinical frontal transformation before and after the operation, respectively. The conspicuous step-off at the inferior orbital rim is clearly visible in the preoperative photograph and appears markedly attenuated in the postoperative one. Preoperative and postoperative worm's-eye perspectives are offered in **Figures 3e and 3f**, respectively, underscoring the regained malar projection.

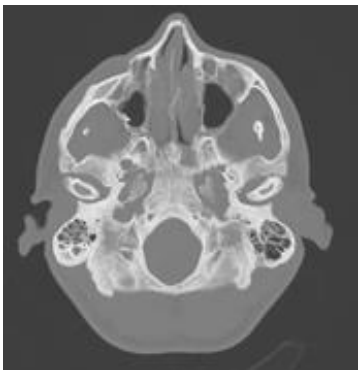

a)

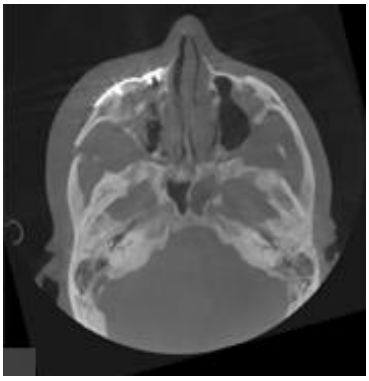

b)

c)

d)

e)

f)

Figure 3. Radiographic and clinical findings: (a) Superimposed preoperative axial CT scans exhibiting a depressed contour of the right zygoma; (b) Superimposed postoperative axial CT scans showing a leveled contour of the right zygoma; (c) Frontal preoperative clinical photograph drawing attention to the step-off defect along the infraorbital rim; (d) Frontal postoperative clinical photograph; (e) Worm's-eye preoperative clinical photograph underscoring the depressed appearance of the right zygoma; (f) Worm 's-eye postoperative clinical photograph.

The same workflow was applied to the patient depicted in **Figure 4**. **Figure 4a** exposes the depressed configuration of the left zygoma after the first operative attempt. **Figure 4b** demonstrates the intended placement of the left zygoma, derived by flipping the right zygoma to serve as a reference model. The seated position of the PSI is captured in **Figure 4c**, while an intraoperative axial CT image confirms the final alignment in **Figure 4d**. **Figure 4e** features the preoperative portrait shot and **Figure 4f** the postoperative equivalent for this individual. A marked volumetric replenishment across the left malar prominence and the infraorbital rim region is clearly discernible in the postoperative image.

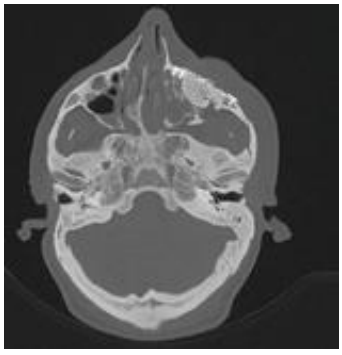

a)

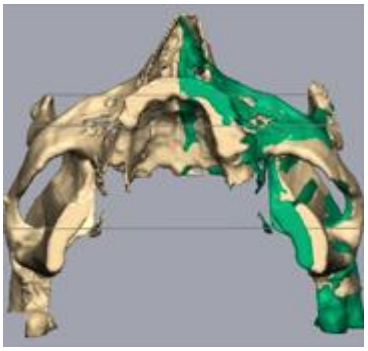

b)

c)

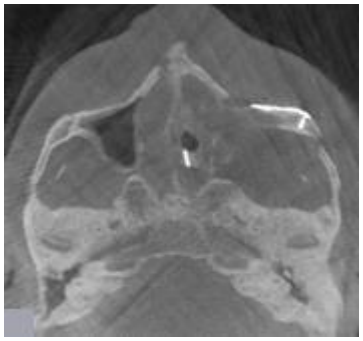

d)

e)

Figure 4. Second case illustration: (a) A composite axial CT view obtained preoperatively, formed by stacking multiple scans into a single 2D image, revealed a depressed left zygoma after a failed earlier surgical procedure; (b) A mirrored representation (green) of the right intact side, flipped to overlay the left compromised side. This mirrored output then acts as a template dictating the optimal placement of the left zygoma; (c) An intraoperative, intraoral capture showing the PSI anchored onto the refractured and freshly realigned

left zygoma; (d) An intraoperative composite axial CT view, constructed from multiple stacked scans, demonstrates harmonized malar landmarks upon securing the PSI; (e) A preoperative frontal clinical view, recorded after the first intervention, highlights recession of the left malar landmark; (f) A postoperative clinical frontal view taken after the subsequent 3D-guided refracture and realignment surgery. Observe the restored contour of the malar landmark.

To objectively assess how closely the simulated operative strategy was replicated, the virtually planned malar position was superimposed on the actual postsurgical result in CloudCompare. A 3D thermal map visualizing this overlay is featured in **Figure 5a**. **Figure 5b** supplies the companion histogram of surface mismatches. The averaged distance separating the planned coordinates from the definitive postsurgical coordinates reached 0.72 mm, with the greatest clustering occurring along both the forward and rearward margins of the malar bone. **Figure 6** juxtaposes the postsurgical malar bone arrangement against its presurgical baseline. The 3D thermal visualization is shown in **Figure 6a**, and the corresponding histogram, reflecting a mean repositioning magnitude of 5.5 mm, is shown in **Figure 6b**. **Figure 7** presents a thermal plot of soft-tissue surface alterations between the preoperative and postoperative configurations across the malar territory. An integrated overlay that fuses the preoperative presentation, the digital surgical plan, and the final postoperative result is shown in **Figure 8**. **Figure 9a** illustrates the three-dimensional displacement trajectory of a single exemplary point located along the infraorbital rim, extrapolated by merging the preoperative and postoperative digital models. **Figure 9b** enumerates that same point's translational values across the X, Y, and Z axes, along with the overall absolute vector magnitude attained.

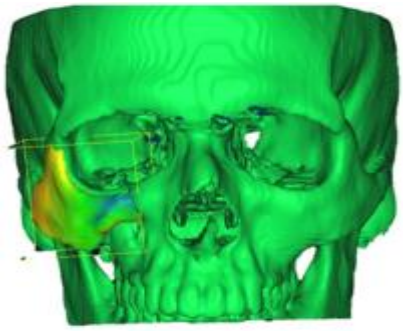

a)

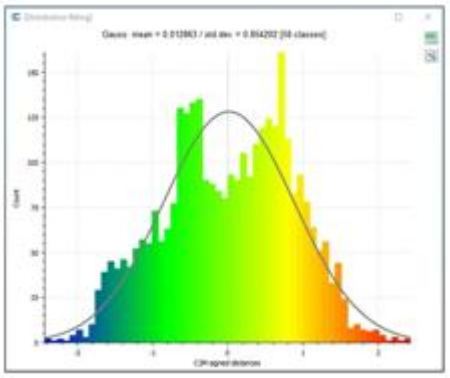

b)

Figure 5. Planned versus postoperative comparison: (a) A thermal map depicting deviations between a three-dimensional reconstruction of the postoperative CT scan and the preoperatively planned zygoma placement. The blue spectrum indicates a more medial orientation, whereas the orange spectrum signifies outward projection; (b) The spread of distances separating the postoperative zygoma position from its preoperatively planned counterpart. The vertical axis shows the number of points in the cloud-mesh software. In contrast, the horizontal axis captures the distance each postoperative CT point lies from its corresponding point in the planned configuration.

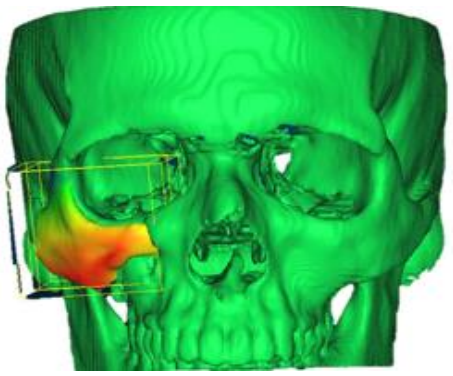

a)

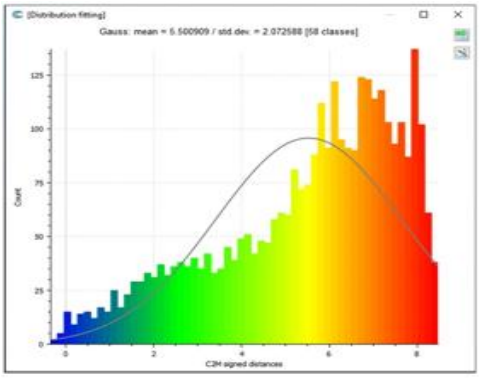

b)

Figure 6. Preoperative versus postoperative comparison: (a) A thermal map illustrating the

discrepancies between a three-dimensional reconstruction of the postoperative CT and the original preoperative zygoma position; (b) The distribution of distances separating the postoperative zygoma placement from its preoperative location. The vertical axis represents the quantity of points registered by the cloud-mesh software, and the horizontal axis indicates the distance each point on the postoperative CT deviates from its corresponding point on the preoperative CT.

a)

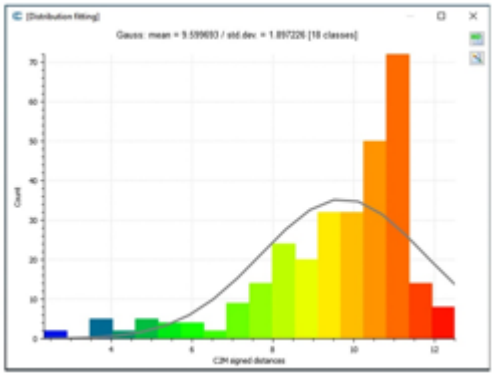

b)

Figure 7. Soft tissue transformation analysis: (a) A thermal map showing the divergence between a three-dimensional reconstruction of the postoperative soft tissue and the preoperative soft tissue; (b) The spread of distances between the postoperative soft tissue configuration and the preoperative soft tissue configuration within the malar territory. The vertical axis shows the total number of points logged by the cloud-mesh software. In contrast, the horizontal axis reflects the gap each point on the postoperative soft-tissue scan exhibits relative to its counterpart on the preoperative scan.

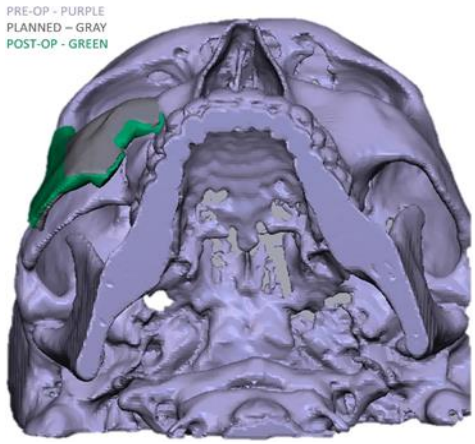

Figure 8. Comparison of the 3D reconstructed zygoma position in the pre-, planned, and post-op CTs.

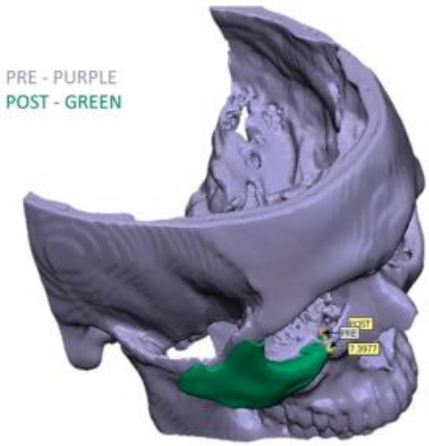

a)

b)

Figure 9. Illustration of quantifying positional shifts along the infraorbital rim: (a) depiction of the displacement experienced by a single point on the infraorbital rim, derived from the preoperative and postoperative three-dimensionally reconstructed models; (b) Quantification of the movement across all three axes, together with the absolute vector distance.

No adverse events occurred in any of the patients who underwent treatment. The average hospitalization duration was 3 days.

The future of medicine lies in individualized, patient-customized care. Among all medical specialties, oncology stands at the forefront of exploring and advancing the concept of personalized treatment, with targeted therapies directed by genomic profiling receiving extensive investigative attention [11]. In the

surgical context, personalized treatment means formulating operative strategies grounded in preoperative imaging data. Surgical planning can be categorized into four distinct tiers. The foundational tier entails merely producing a printed replica of the current anatomical state and basing the operative scheme upon that physical model [12]. The second tier advances further by enabling alterations to the existing anatomical arrangement—for instance, performing a virtual fracture reduction—and subsequently printing the corrected version, which allows for pre-bending of plates and other preparatory steps ahead of the actual intervention [13]. The third tier encompasses the conceptualization of surgical templates, such as reduction guides for accurate alignment and cutting jigs for osteotomies and resections [13]. Occupying the summit of this hierarchy, the fourth tier involves the design and additive manufacturing of patient-specific implants. This level of sophistication enables positioning, reconstruction, and reduction with an exceptional degree of exactitude [10, 14-16]. In this work, we have chronicled the deployment of this fourth-level three-dimensional planning methodology for the correction of a displaced malar bone. Execution relies on surgical guides that serve the dual purpose of directing osteotomy cuts and locating drill perforations necessary for precise realignment, followed by the creation of customized implants that deliver the ultimate fixation. The deployment of a surgical guide for executing the posterior osteotomy through the zygomatic arch makes a precise intra-oral route feasible, thereby rendering an extensive and aesthetically objectionable coronal dissection unnecessary. A further consideration that facilitates avoiding coronal access is the remarkable precision with which the PSI repositions the malar bone. Attempting to restore this osseous structure to its correct spatial location without a PSI would require extensive operative exposure. The technique articulated here is equally applicable to the management of malpositioned bones elsewhere in the body. It is relevant to the disciplines of orthopedics, maxillofacial surgery, ENT, plastic surgery, and neurosurgery. Once the approach had been put into practice, it became necessary to devise a rigorous analytical framework for its appraisal. Assessment was undertaken within the CloudCompare platform, following processing of the malar bone and isolation of its outer cortical contour to prevent analytical misinterpretation. This protocol was used to assess the superimposition accuracy of both hard and soft tissues using the Hausdorff distance. The outcomes reveal robust concordance between the three-dimensionally planned configuration and the surgically realized, stabilized position upon 3D spatial analysis, with a mean deviation of only 0.72 mm, concentrated largely at the anterior and posterior junctions of the segmented bony fragment **(Figure 5)**. It deserves emphasis that the patient-specific fixation plates were manufactured for merely one articulation uniting the repositioned malar bone with the adjoining stationary skeleton, even though the zygoma is known to articulate at four separate junctions. Had an additional articulation been secured with another PSI, it is reasonable to surmise that the degree of precision would have been further elevated. In certain instances within this category, patients may have undergone several prior surgical attempts, and bone substance may be deficient—most notably along the anterior wall of the maxillary sinus—thereby prompting the design of a plate of greater dimensions. This circumstance can lead to patient discomfort if the plate boundary coincides with the malar prominence. One must keep in mind that PSI plates inherently possess superior structural integrity compared with standard plates, as they are not subjected to manual intraoperative contouring; consequently, even in areas of bone loss, overly thick plate designs should be avoided. That caveat notwithstanding, it is advisable not to locate screw perforations excessively far back on the zygomatic body, as the operative window achievable through an intra-oral approach will be constrained by soft tissue retraction. Judicious consideration must be accorded to striking an equilibrium between the goal of reconstituting the malar eminence and the imperative to avert unintentional augmentation of orbital volume. Such volumetric expansion can manifest in the sphenozygomatic region as a sequela of prior comminution. It may be inadvertently exacerbated when the segment is deliberately rotated during the virtual planning phase to highlight the malar point better. The anterior maxillary sinus wall should be deliberately excluded as a fixation site for the PSI. Recognizing that the three-dimensional spatial positioning of the zygoma is paramount, employing two separate PSIs to secure the bone in its intended new location will yield superior positional fidelity compared with relying on a single implant. Exercising caution to preserve the infraorbital nerve during anterior segmentation is imperative; this objective demands precise, meticulous contouring of the infraorbital canal.

The cases elaborated in this manuscript were planned internally by the attending surgical team, utilizing the software platforms specified herein. There is the option of contracting external commercial entities to perform

the planning, a choice that comes with distinct benefits and limitations. Reliance on outside firms engenders considerable cost escalation, prolongs the timeline to definitive treatment, and diminishes the surgeon's preparedness, as they remain less intimately aware of any case-specific anatomical complexities or obstacles encountered during the design process. On the other hand, outsourcing substantially reduces the temporal commitment required of the surgeon for case preparation, select companies possess deep reservoirs of expertise—particularly in well-established interventions like orthognathic procedures—and it removes the need to purchase and maintain 3D design software infrastructure.

Conclusion

We assert that integrating three-dimensional planning with patient-specific implants for secondary refracturing and reconstruction of a malpositioned malar bone constitutes a remarkably precise and predictable strategy, one that substantially curtails the impact of human fallibility in these technically demanding cases. It is our conviction that every practitioner in craniomaxillofacial surgery ought to be acquainted with this therapeutic avenue, irrespective of whether the planning is undertaken within the surgeon's own department, as illustrated by our experience, or entrusted to an external service.

Acknowledgments: None

Conflict of Interest: None

Financial Support: None

Ethics Statement: The Rambam Health Care Campus Institutional Ethical Review Board approved the studies involving humans. The studies were conducted in accordance with the local legislation and institutional requirements. Written informed consent for participation was not required from participants or their legal guardians/next of kin, in accordance with national legislation and institutional requirements. Written informed consent was obtained from the individual(s) for the publication of any potentially identifiable images or data included in this article.

References

1. Becelli R, Carboni A, Cerulli G, Perugini M, Iannetti G. Delayed and inadequately treated malar fractures: evolution in the treatment, presentation of 77 cases, and review of the literature. Aesthetic Plast Surg. 2002;26(2):134-8.
2. Dorafshar AH, Rodriguez ED, Manson PN. Facial Trauma Surgery E-Book: From Primary Repair to Reconstruction. Amsterdam: Elsevier Health Sciences; 2019.
3. Hooley JR, Freedman G. Delayed treatment of a fracture of the zygomatic complex: report of a case. Oral Surg Oral Med Oral Pathol. 1967;24(5):585-8.
4. He Y, Zhang Y, An JG, Gong X, Feng ZQ, Guo CB, et al. Zygomatic surface marker-assisted surgical navigation: a new computer-assisted navigation method for accurate treatment of delayed zygomatic fractures. J Oral Maxillofac Surg. 2013;71(12):2101-14.
5. Feng F, Wang H, Guan X, Tian W, Jing W, Long J, et al. Mirror imaging and preshaped titanium plates in the treatment of unilateral malar and zygomatic arch fractures. Oral Surg Oral Med Oral Pathol Oral Radiol Endod. 2011;112(2):188-94.
6. Gong X, He Y, An J, Yang Y, Huang X, Liu M, et al. Application of a computer-assisted navigation system (CANS) in the delayed treatment of zygomatic fractures: a randomized controlled trial. J Oral Maxillofac Surg. 2017;75(7):1450-63.
7. Lassausaie A, Sesqué A, Barthélémy I, Depeyre A. Virtual surgery planning and three-dimensional printing template for osteotomy of the zygoma to correct untreated zygomaticomaxillary complex fracture. J Craniofac Surg. 2020;31(4):1142-5.
8. Aman HM, Alenezi A, Ducic Y, Reddy LV. Secondary reconstruction of the zygomaticomaxillary complex. Semin Plast Surg. 2020;34(4):254-9.
9. Li P, Tang W, Li J, Tian DW. Preliminary application of virtual simulation and reposition template for zygomatico-orbitomaxillary complex fracture. J Craniofac Surg. 2012;23(5):1436-9.
10. Krasovsky A, Hija A, Zeineh N, Capucha T, Haze DA, Emodi O, et al. Comparison of patient specific implant reconstruction vs conventional titanium mesh reconstruction of orbital fractures using a novel method. J Craniomaxillofac Surg. 2024;52(4):491-502.
11. Murciano-Goroff YR, Taylor BS, Hyman DM, Schram AM. Toward a more precise future for oncology. Cancer Cell. 2020;37(4):431-42.
12. Hull CW. Apparatus for production of three-dimensional objects by stereolithography. US patent 4575330A. 1986.
13. Shilo D, Capucha T, Krasovsky A, Blanc O, Emodi O, Haze A, et al. Real-time reconstruction

of comminuted mandibular fractures using 3D printing. Plast Reconstr Surg Glob Open. 2024;12(3):e5645.

14. Capucha T, Shilo D, Blanc O, Turgeman S, Emodi O, Rachmiel A. 3D planning and printing of patient specific implants for reconstruction of bony defects. J Vis Exp. 2020;(162):e60929.
15. Shilo D, Capucha T, Blanc O, Shilo Yaacobi D, Emodi O, Rachmiel A. Patient-specific implants for treating atrophic mandibles. Plast Reconstr Surg Glob Open. 2022;10(6):e4359.
16. Shilo D, Capucha T, Goldstein D, Bereznyak Y, Emodi O, Rachmiel A. Treatment of facial deformities using 3D planning and printing of patient-specific implants. J Vis Exp. 2020;(159):e60930.